

Hydrodynamic Model Analysis of an Idealized Bosphorus Case with respect to Switching Steady-State Solutions

Adil SÖZER^{1,2*}, Emin ÖZSOY²

^{1*}Fatsa Faculty of Marine Sciences, Ordu University, Ordu, Turkey

²Institute of Marine Sciences, Middle East Technical University, Mersin, Turkey

(Received Date/ Geliş Tarihi: 13.05.2019; Accepted Date/ Kabul Tarihi: 29.05.2019)

Abstract

Hydrodynamics of the Bosphorus Strait is examined with a three-dimensional ocean model under the idealized conditions, while solving the full set of the primitive equations for the simplified hydrography and geometry of the strait. The response of the idealized model switching from one steady-state to another, from a less frictional case to a more frictional one or vice versa are investigated. The results show that the model is successful in switching from a less frictional state to a more frictional one, but has difficulties in the opposite direction. Inconsistency between the reservoir stratification partly defined by the initial condition and the maximal-exchange characteristic of the steady-state solution of the restarted simulation prevents a successful switch from a well-mixed case to a reduced mixing solution.

Keywords: Idealized Bosphorus Strait; Hydrodynamic modeling; Maximal-exchange

1. Introduction

The Turkish Straits System (TSS) provides a restricted connection between the two large inland seas of the Black Sea and the Mediterranean, Figure 1a. It has extremely complex geometry with irregular coastlines where the Sea of Marmara is connected to the Black and the Aegean Seas through the Bosphorus and the Dardanelles straits. With a sharp pycnocline at 25 m separating water masses of Black Sea and Mediterranean Sea origin, TSS has a permanent two-layer stratification (Andersen & Carmack 1984; Ünlüata et al 1990), where the upper-layer displays a seasonal response and the relatively more uniform lower-layer buffers inputs from the Aegean Sea (Beşiktepe et al 1993; 1994; 2000).

The Bosphorus is a narrow strait connecting Black and the Marmara Seas with a total length of ~35 km and an average width of 1.3 km at the surface, corresponding to a distinctive aspect ratio. The strait bathymetry displays great variability in both the along-channel and the cross-channel directions with a maximum depth of ~105 m coinciding with the narrowest section (700m surface width) located at about one-third of the length of the strait from the southern end, Figure 1b. This contracted region, a sill located at ~3.5 km north of the Marmara junction and the northern sill lying on the 'pre-Bosphorus channel' extending onto the Black Sea continental shelf are the three important topographic elements of the Bosphorus Strait. In addition to these three geometrical features, the two main bends of the channel in the northern half of the strait and the abrupt opening to the Marmara Sea in the south are important geometric details of the channel.

*Sorumlu Yazar/ Corresponding Author: adilsozer@gmail.com, <https://orcid.org/0000-0002-8674-1461>
Emin ÖZSOY: ozsoy@ims.metu.edu.tr, <https://orcid.org/0000-0002-1519-0471>

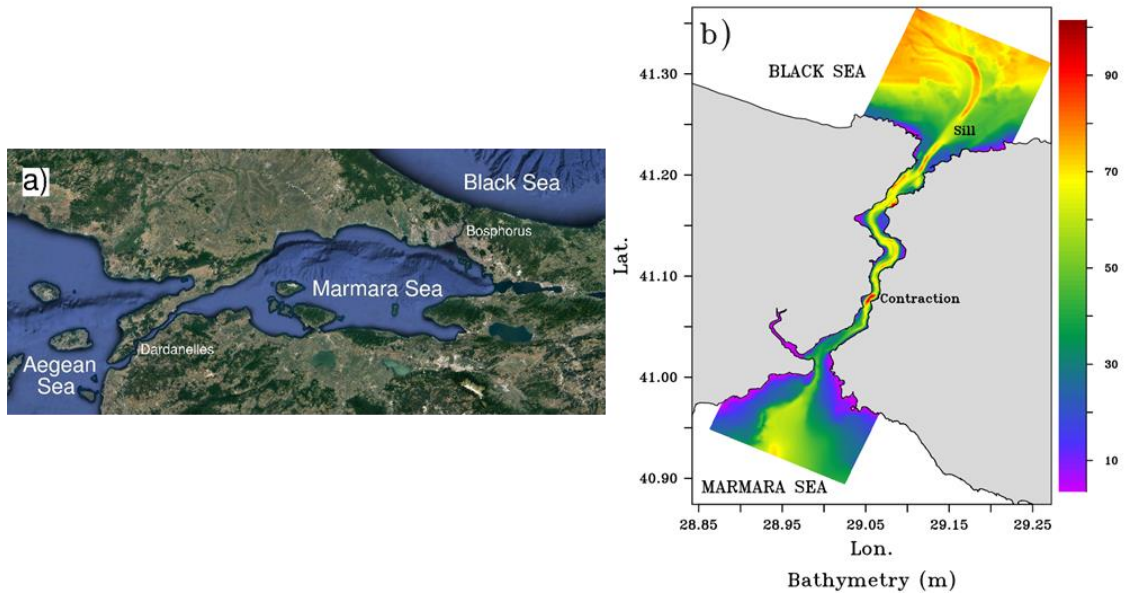


Figure 1. a) Location map for Turkish Straits System from Google Earth and b) bottom topography of the Bosphorus Strait.

The Bosphorus strait is the most constricted element of the TSS, and has the most significant role in the two-layer exchange between the Mediterranean and the Black Seas. Apart from all its topographical and geometrical complexities, the contraction and the north sill, the sill being located on the side of the less dense reservoir, has a combined effect making the two-layer exchange through the Bosphorus strait is ideally suited to the support the 'maximal-exchange' regime with due to suitable reservoir conditions, Farmer and Armi (1986).

The transfer through the Bosphorus is basically driven by the hydrostatic pressure difference resulting in the dense water flow from Marmara to the Black Sea in the lower layer and surface flow of lighter water in the opposite direction. The existence of the undercurrent was first explained and verified experimentally by Marsigli (1681), considered to be the first remarkable contribution to oceanography in history and has been honored in the modern age (Defant 1961; Soffientino & Pilson, 2005; Pinardi 2009). The direction of the net barotropic flow is towards the Marmara Sea due to the mean excess of fresh water inputs of the Black Sea, resulting in a superior sea-level on the Black Sea side.

The two-layer stratification roughly defined by a sharp pycnocline descending from the surface at the south-exit towards the bottom at the north sill. On the southern end, in the lower-layer, Marmara Sea possesses constant properties with average temperature and salinity values of 14.5 °C and 38.5 respectively, filling the basin below the halocline, located at a relatively constant depth of 25 m. The upper-layer exhibits seasonal variability with salinity values of 23 ± 2 and temperature values between 7 °C and 22 °C, with higher salinity and lower temperature occurring in winter as a result of cooling and wind driven mixing, as well as decreased inflow from the Black Sea (Ünlüata et al 1990; Beşiktepe et al 1994). On the Black Sea side, the surface salinity is related to the fresh water flux and estimated to vary within 17.5 ± 2 by Çetin (1999) for the period 1992-1998, in agreement with the results of the Özsoy & Ünlüata (1997) for the southwestern

Black Sea during 1986-1992. The surface temperature varies seasonally by surface heating and cooling, dropping to about 4 °C at the surface in winter and reaching to about 25 °C in summer (Ünlüata et al 1990), overlying CIL with core temperatures of ~6.5 °C typically between 25 - 100 m depth at the northern boundary of the strait. These properties at the entrance to the Bosphorus from Black Sea influence salinity and temperature variations through the strait (Ovchinnikov & Popov 1991; Altıok et al 2012; Özsoy et al 2001; Sözer 2013).

Hydraulic adjustments at the three topographic constrictions; north-sill, the contraction and the south-exit, results in abrupt changes with non-linear dynamics in the strait flow as demonstrated schematically in Özsoy et al (1998). The violent and sudden changes occur downstream of these controls, as reported by various observations (Latif et al 1991; Özsoy et al 2001; Gregg & Özsoy 2002) and confirmed by modeling (Sözer 2013). Within the southern part of the strait, from south-exit to contraction with quite complicated geometry and bathymetry, the interface thickens and increased mixing is observed in the upper part of the flow. Similar response is observed in the lower layer flow past the north sill, while almost linear variation occurs in the depth of the thin interface between these two sections. The variation of the zero-velocity surface through the channel is in agreement with the density interface, but stays above the density interface at the northern exit and lies below it at the southern part of the strait, as proposed by Tolmazin (1985), shown by Gregg & Özsoy (2002) and verified with a three-dimensional model by Sözer (2013).

Considering that salinity change with depth is rather small in the Black Sea opening of the Bosphorus strait, and with relatively uniform properties of the lower layer in the Marmara Sea, the most prominent effect on the strait flow is the seasonal change in mixed-layer temperature in response to heating and cooling on the Black Sea side. A very rough estimation for the density difference between the lower layer of the Marmara Sea with almost constant properties and the water column at the Black Sea exit would be ~16 kg/m³ for the winter months with close values to the summer conditions which is ~2 kg/m³ larger despite the decrease in salinity due to the very effective seasonal heating/cooling in the Black Sea region.

The excess fresh water inflow into the Black Sea given by Precipitation (P) + River Runoff (R) - Evaporation (E) is estimated as $300 + 352 - 353 = 300$ km³/yr, balanced by the net volume-flux through the Bosphorus. The annual mean upper and lower layer fluxes are estimated by steady-state salt and mass conservation equations, yielding ~600 and ~300 km³/yr respectively (Ünlüata et al 1990). However, the net volume flux through the Bosphorus obviously varies seasonally, with maximum values from March and April and minimum in August, Peneva et al (2001). Following the mass budget technique of Ünlüata et al (1990) while utilizing improved estimates of fresh water inflow mainly from Danube, Tuğrul et al (2002) estimated the seasonal flux variations of the Bosphorus with mean annual values consistent with Ünlüata et al (1990). Mean volume-flux estimates by ADCP direct velocity measurements, Özsoy et al (1996) and (1998), demonstrates great variability with increased volume-fluxes from winter to spring and decreased estimates from late summer to autumn, in agreement with the results of Peneva et al (2001). Mean volume-fluxes obtained by ADCP measurements are found be 540 km³/yr and 115 km³/yr for the upper and lower layers respectively, resulting in considerably larger barotropic transport compared to previous mass balance estimates, possibly by loss of data very close to the bottom. The instantaneous values

reach much larger values of $\sim 1600 \text{ km}^3/\text{yr}$ and $\sim 650 \text{ km}^3/\text{yr}$ respectively for the upper and lower layers, as confirmed by other direct measurements, Altıok et al (2010) and Jarosz (2011). The instantaneous net barotropic volume transport through the Bosphorus is quite variable with much larger values than the mean seasonal values, the transient variability in the Bosphorus flow system mainly results from meteorological events within the TSS region with time-scales ranging from a few hours to 10 days; Ünlüata et al (1990), Büyükay (1989), Gunnerson & Özturgut (1974).

In this study, hydrodynamics of the Bosphorus Strait is examined with a three-dimensional ocean model under the idealized conditions, while solving the full set of the primitive equations for the simplified hydrography and geometry of the strait. Similar models have already been developed to understand the dynamics of the Bosphorus flow (Sözer & Özsoy 2002; Oğuz 2005). More recent modeling studies have been successfully implemented utilizing the realistic topography of the Bosphorus Strait (Öztürk et al 2012; Sözer & Özsoy 2017) and covering the complete TSS domain (Sannino et al 2017; Aydoğdu et al 2018) or neighboring Aegean and Black Seas (Stanev et al 2017). In particular, here we examine the idealized model's ability in switching from one steady-state solution to another which differentiate only in terms of the mixing strengths either in vertical or horizontal direction.

2. Material and Methods

2.1 Numerical Model, ROMS

ROMS (www.myroms.org) is a free-surface, terrain-following, primitive equation, open source community ocean model written in F90/F95 with a modular structure and very popular in the scientific community with wide range of applications; Haidvogel et al (2000), Wilkin et al (2005) and Hedström (2009). The model is a successor of SCRUM introduced by Song & Haidvogel (1994). Various sub-models for biogeochemical (Fennel et al 2006), sedimentary (Warner et al, 2008) and sea-ice (Budgell 2005) are optionally available in ROMS. The code can be run in serial mode but also includes very efficient parallelization options with domain partitioning.

The model solves the Reynolds averaged Navier-Stokes equations, under the hydrostatic and Boussinesq approximations on orthogonal curvilinear/rectilinear coordinates with an Arakawa "C" grid arrangement (Arakawa & Lamb 1977) in the horizontal while utilizing a stretched topography following vertical coordinate system discretized with a staggered vertical stencil in the vertical direction. In addition to the availability of boundary fitted curvilinear grids, land/sea masking of the horizontal grid points enables coastal applications with irregular coastlines. Free-slip or no-slip boundary conditions can be set for the tangential velocity components on the lateral surface of the masked cells or in the vicinity of lateral open boundaries set to "wall boundary" conditions. Various methods for the treatment of open boundaries are readily available in the model code. Such as the Orlanski radiation boundary condition where a local phase speed normal to and outwards from the boundary is used to radiate the waves out which is originally developed in one direction, Orlanski (1976) and further extended to include all three directions by Raymond and Kuo (1984), but implemented in only two horizontal directions in ROMS.

Bottom stress at the sea floor can be defined as linear, quadratic, or logarithmic terms. The surface boundary condition for the salinity is a function of evaporation and

precipitation, while the surface heat flux is computed from the surface temperature and the atmospheric fields via the use of atmospheric bulk flux routine which is also utilized for the computation of the surface wind stress from the wind data. As in the case of surface, it is possible to set a flux value for the scalar quantities at the bottom, which is generally set to zero in most of the applications, Hedström (2009). Indeed, in idealized simulations performed in this study, all vertical fluxes except the bottom stress are set to zero.

The presence of a free-surface imposes a more severe time-step than any of the internal processes, therefore numerical solution is performed by coupling the external mode, depth integrated, and the internal mode, vertically varied, equations where full set of the equations are solved by means of a split time-step method while a short time-step is used in the integration of the external mode, Hedström (2009).

The strength of the Laplacian and biharmonic horizontal viscosity and diffusion can be defined by predefined constants or by the horizontal shear dependent Smagorinsky method (Smagorinsky 1963) utilized for the computation of eddy harmonic and biharmonic constants, (Griffies & Hallberg 2000). However, horizontal viscosity and diffusion acting along constant s -surfaces (topography following surfaces) is often not satisfactory and may lead to spurious vertical mixing in the presence of sharp topography, therefore ROMS has the option of rotated mixing tensors for the Laplacian and biharmonic operators which provide options for mixing on constant geopotential surfaces and constant in-situ density surfaces in addition to the horizontal mixing on constant s -surfaces. In addition to the simplest definition of vertical viscosity and diffusion in the form of fixed constants, various types of local, Mellor & Yamada (1982) and Generic Length Scale (GLS) parametrization (Umlauf & Burchard 2003), or nonlocal, K-Profile boundary layer formulation by Large et al (1994) including surface and oceanic boundary layers, are implemented in the source code for the definition of the vertical mixing. The comparison of these methods can be found in many studies such as Warner et al (2005) and Durski (2004).

ROMS is a constantly developing multi-purpose ocean model project supported by a large community, therefore it is not possible to give a complete coverage of the model abilities here, but further details such as the numerical solution technique and coordinate transformation can easily be followed from the available online sources.

2.2 Idealized Model

2.2.1 Model Grid

The geometry of the Bosphorus Strait is idealized with a contracting channel, ~34 km in length and 1300 m in width, which has a 4 km long symmetric contraction lying at one-third of its length from the south end of the channel with a width of 700 m at the narrowest section, Figure 2. The abrupt openings to the Marmara and the Black Seas are adjoined with two relatively large reservoirs. A sill with Gaussian shaped topography, 1 km in length, extends in the north-south direction where the channel joins the northern reservoir. The bottom is otherwise flat with a constant depth of 70 m excluding the sill region which has a crest height of 13 m above the flat bottom. The model domain is discretized on a 55*512*35 rectilinear grid, where $dx=100$ m and $dy=100$ m. There are 35 topography following vertical s -levels resulting in a vertical resolution of 1.6-2.0 m. The channel geometry is outlined by land masking of the grid cells and lateral

boundaries of the model grid are defined by two masked grid sections in east and west sides approaching a width of 5100 m in both reservoirs. Although the Bosphorus Strait geometry is too complex for a simplified representation, we minimally represent its most significant features in the idealized model, keeping elements with a primary influence on the exchange flows: these are the contraction, the north sill and the south-exit, with realistic dimensions.

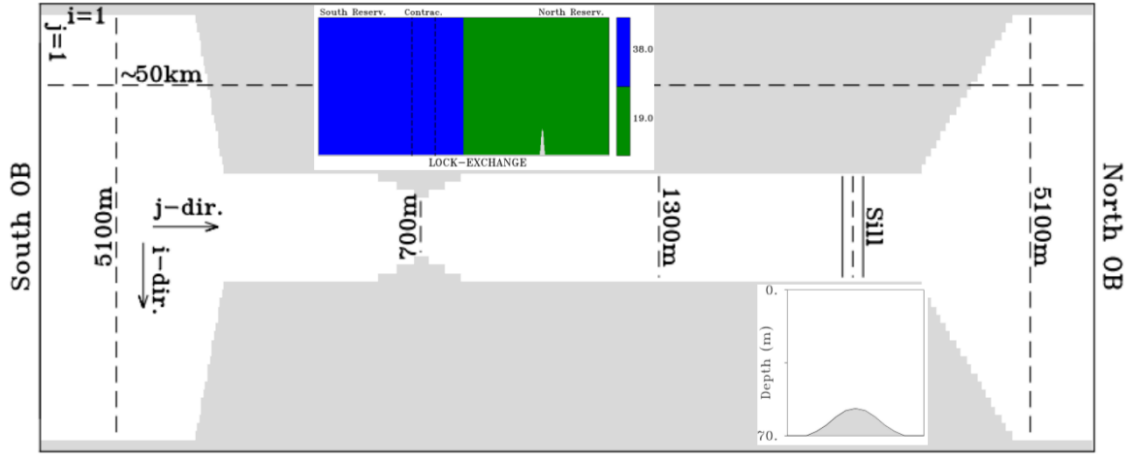


Figure 2. Layout of the idealized Bosphorus Model and the demonstration of the Lock-Exchange (LE) initial condition (top insert).

2.2.2 Initial Conditions

The baroclinic flow in the strait is allowed to develop from simple hydrographic conditions which are initially at rest: the model is started from a lock-exchange (LE) initial condition consisting of water masses with contrasting salinities filling the north and south reservoirs and meeting at mid-channel, while the temperature is taken out of the nonlinear equation of state used in the model. Since the strong salinity gradient has greater contribution to the density difference between the two ends of the strait, while lowering the computational cost. The LE initial condition shown in Figure 2, having salinity values of 38.0 and 19.0 at south and north respectively corresponds to an initial density difference of 14.6 kg/m^3 .

2.2.3 Physical and Numerical Setup

Within the scope this study, numerical simulations are performed around a central run, which will be called as “BASE” in the rest of the text. The configuration for this BASE simulation is summarized below.

Laplacian mixing in the vertical, and along constant geopotential surfaces in the horizontal are assumed, with eddy mixing constants of $K_v=0.0001 \text{ m}^2/\text{s}$ and $K_h=15.0 \text{ m}^2/\text{s}$ respectively for both momentum and salinity. The three-dimensional variables are radiated at the open boundaries while the two-dimensional variables are treated according to the gradient boundary condition, except for the south-north component depth averaged velocity which is clamped at the south edge resulting in a net volume-flux of $3500 \text{ m}^3/\text{s}$ from the north to the south, a comparable value with the actual mean annual value of $\sim 10000 \text{ m}^3/\text{s}$ from the Black Sea to the Sea of Marmara (Ünlüata et al, 1990). No-slip boundaries are assumed at the side-walls, while a quadratic bottom

friction with $RDRG2=0.005$ is implied at the bottom. Considering that the internal Rossby Radius of Deformation is significantly larger than the channel and the reservoir widths in the model, the rotation of the earth is ignored. Due to the sharp gradients of salinity maintained in the model, the recursive MPDATA advection scheme (Smolarkiewicz 2006) is selected to prevent over/under shooting in the salinity field and defaults schemes are utilized for 2d and 3d momentum. The model is started from the LE initial condition with a considerably small baroclinic time-step of 3.5 seconds and a 20 times smaller barotropic time-step (to ensure stable integrations) for a total duration of ~ 1 day.

The use of a constant net volume-flux without the time-dependent effects clearly is a great simplification of the physical system, limiting the solution to the steady-state case. However, this approximation only and optimistically searches for the steady-state solution for a constant net volume-flux through the channel, while providing the resultant free-surface response corresponding to the specified net barotropic flux and density difference.

2.3 State Switching Simulations

In this study, the response of the idealized model switching from one steady-state to another, from a less frictional case to a more frictional one or vice versa are investigated. A total of 11 simulations, including the central simulation (BASE), is performed (tabulated in Table 1). Experiments starting from the LE initialization with different K_h and K_v combinations (centered around the BASE simulation) given in the first five rows of the table. The following six state switching simulations in the table are named as; BASE= \Rightarrow HVM, BASE= \Rightarrow LVM, HVM= \Rightarrow BASE, BASE= \Rightarrow HHM, BASE= \Rightarrow LHM and HHM= \Rightarrow BASE. A self-explanatory naming method is used in all of the experiments with the naming convention explained in the second column of the table. Cumulative duration of the simulations are 1.01 days for the LE experiments and 2.02 days for the restarted cases. Five LE initialized experiments and the following six state switching simulations tabulated in the table have exactly the same physical and numerical configurations except for the Laplacian constants or/and the initial conditions.

Briefly, there are two groups of simulations presented in the Table 1, the first group consists of 5 simulations starting from a LE initial condition while the following six cases belonging the second group are the restarted solutions initialized from the final states of the three simulations (BASE, HVM and HHM) of the first group. The second group is divided into two subsets; the first three simulations with increased/decreased vertical mixing and the last three cases with increased/decreased horizontal mixing.

Table 1. Summary of the switching state solutions with different horizontal and vertical mixing strengths, LE refers to lock-exchange initialization.

	Simulation	Explanation	Initial Condition	K_h (m²/s)	K_v (m²/s)
LE Solutions	BASE	Central Run	LE	15	10 ⁻⁴
	HVM	High Vert. Mix.	LE	15	10 ⁻³
	LVM	Low Vert. Mix.	LE	15	10 ⁻⁵
	HHM	High Hor. Mix.	LE	45	10 ⁻⁴
	LHM	Low Hor. Mix.	LE	5	10 ⁻⁴
Restarted Solutions	BASE=>HVM	To High Vert. Mix.	BASE	15	10 ⁻³
	BASE=>LVM	To Low Vert. Mix.	BASE	15	10 ⁻⁵
	HVM=>BASE	To Low Vert. Mix.	HVM	15	10 ⁻⁴
	BASE=>HHM	To High Hor. Mix.	BASE	45	10 ⁻⁴
	BASE=>LHM	To Low Hor Mix.	BASE	5	10 ⁻⁴
	HHM=>BASE	To Low Hor. Mix.	HHM	15	10 ⁻⁴

3. Results and Discussion

The following discussion of the results is mainly based on the comparison of the resultant along-channel salinity, along-channel velocity (v-velocity) responses of the restarted solutions with the LE initialized equivalents and also includes comparison of layer fluxes and the two-layer Froude-number responses estimated from the layer averaged properties defined by the zero-velocity surface.

For the first subset of the experiments the model is restarted with an increased or decreased vertical mixing coefficient (K_v). Comparison of these restarted solutions (BASE=>HVM, BASE=>LVM and HVM=>BASE) with the LE initialized equivalents (HVM, LVM and BASE) in terms along-channel salinity, velocity, layer fluxes and Froude-number responses at the final state of the solutions are given in Figure 3. For these three restarted simulations, the model successfully adjusts the thickness and the slope of the interface according to the vertical mixing constant used and resulted in similar results which are almost exactly the same in terms of salinity and velocity

responses with the equivalent LE initialized solution within the region from the south-exit to the sill. Despite minor differences between the switched and the LE solutions within the reservoirs, the along-channel volume-flux response of the layers and the along-channel response of the layer Froude-numbers are almost identical within the inner channel. Discrepancies observed within the reservoirs is partially due to the interaction of the initial level of the salinity interface at the reservoirs with the open boundary conditions. Since there is only a radiation condition for the salinity and the along-channel 3d velocity field at the open boundaries, the model ensures to enforce upstream conditions at the boundaries, specifying the internal value during outflow and persisting the interior values whenever an inflow exists. However, the initialization cannot be held completely responsible for these differences, especially for the cases BASE=>LVM and HVM=>BASE in which the model has already problems in dealing with the fast very thin outflows of upper and lower layers at the reservoirs. Numerical instabilities within these regions are apparent from the noisy behavior of the along-channel sections, but the model can be safely considered as quite successful in switching from one state to another regardless of the direction of change; either towards the less or the more frictional state.

For the second subset of the restarted solutions where horizontal mixing is changed, (BASE=>HHM, BASE=>LHM, and HHM=>BASE) the results are direction dependent. The case BASE=>HHM where the BASE solution is forced to a state with a larger K_h , the solution is equivalent with the LE initialized equivalent (HHM) as in the case of the first subset demonstrating perfect agreement within the channel and minor differences at the boundaries, Figure 4. For the other two experiments where model is forced from a higher to lower frictional state, the salinity response within the reservoirs is distinctively different than the LE initialized equivalents, and although the velocity response within the reservoirs is quite noisy, a clear deficiency between the switched and the LE solution is observed. The difference between the switched and the LE equivalent solution is not limited to the salinity stratification within the reservoirs but also slightly different salinity and velocity responses are observed within the channel probably due to the increased thickness of the salinity interface at the boundaries. In agreement with the difference in along-channel velocity response, layer fluxes of the switched solutions are also less than the LE equivalents due to the decreased density difference between the reservoirs. However, the similarity of the along-channel interface and the Froude-number responses between the switched and the LE solutions suggests that the hydraulic responses from south-exit to sill are similar to each other with existing controls at the south-exit and at the sill. The upper-layer control is very clear at the south-exit for both of the switched solutions, but not recognizable at the sill with estimations of $F^2_2 < 1.0$ which is also lower than the LE equivalent counterparts. However, estimations of F^2 based on the layer averaged properties defined by the zero velocity surface is quite conservative, but a two-layer sense of control at the sill for these two solutions is apparent from the two-dimensional response of the energy corrected (M_3 corrected, Sözer & Özsoy 2017) responses of F^2_2 over the sill as demonstrated in Figure 5.

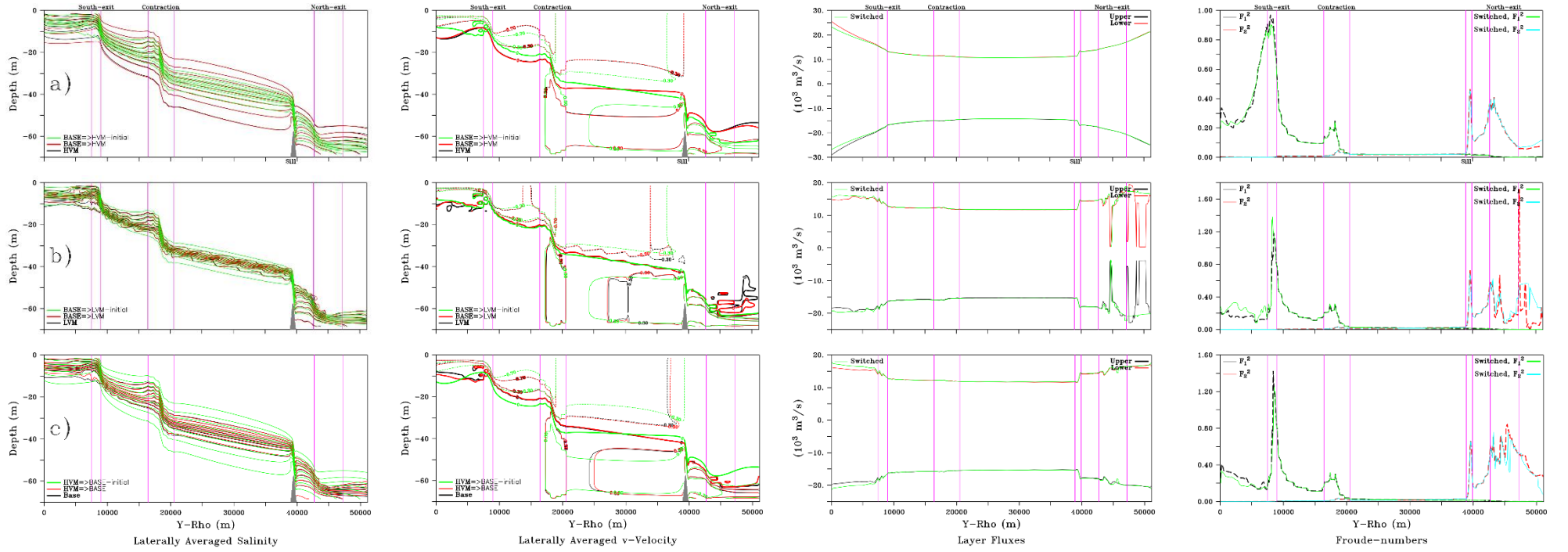


Figure 3. Comparison of the along-channel responses for the laterally averaged salinity, v-velocity, layer fluxes and F^2 defined by the zero velocity surface between the LE equivalent cases and the switched state solutions; a) BASE=>HVM vs HVM, b) BASE=>LVM vs LVM and c) HVM=>BASE vs BASE, in the contour plots (with the very same levels for the three colors) LE equivalent solution is demonstrated by black color, the initial condition of the switched experiment and the corresponding solution are given by green and red colors respectively; for flux responses, LE equivalent solution is demonstrated by black (Q_1) and red (Q_2) lines and the switched solution is plotted in green color; F_1^2 (black) and F_2^2 (red) are given by dashed lines for the LE equivalent case, while the switched solution responses are given by green (F_1^2) and light blue (F_2^2) colors, location of the topographic changes are marked with purple lines. Subscripts, 1 and 2 corresponds to upper and lower layers respectively.

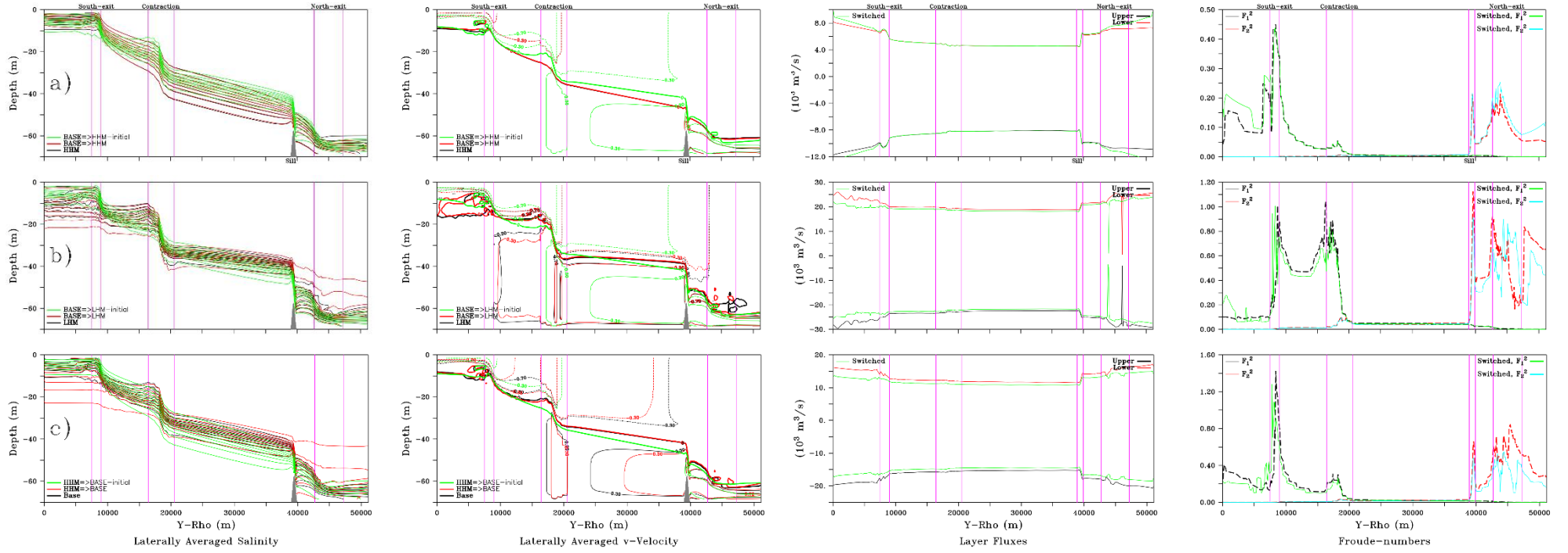


Figure 4 . Comparison of the along-channel responses for the laterally averaged salinity, v -velocity, layer fluxes and F^2 defined by the zero velocity surface between the LE equivalent cases and the switched state solutions; a) BASE=>HHM vs HHM, b) BASE=>LHM vs LHM and c) HHM=>BASE vs BASE, in the contour plots (with the very same levels for the three colors) LE equivalent solution is demonstrated by black color, the initial condition of the switched experiment and the corresponding solution are given by green and red colors respectively; for flux responses, LE equivalent solution is demonstrated by black (Q_1) and red (Q_2) lines and the switched solution is plotted in green color; F_1^2 (black) and F_2^2 (red) are given by dashed lines for the LE equivalent case, while the switched solution responses are given by green (F_1^2) and light blue (F_2^2) colors, location of the topographic changes are marked with purple lines. Subscripts, 1 and 2 corresponds to upper and lower layers respectively

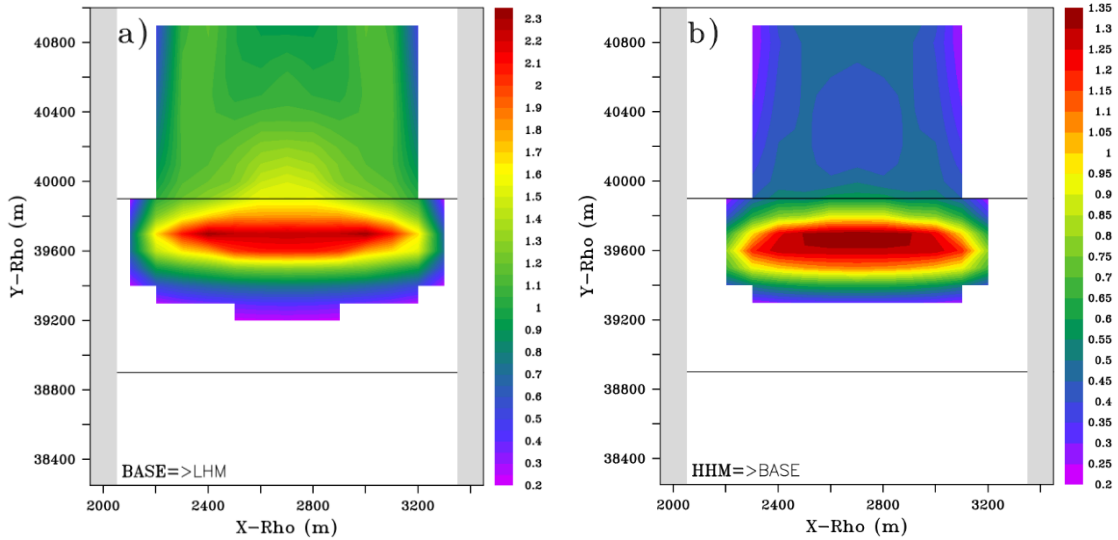


Figure 5. Two-dimensional variation of energy corrected F_2^2 (lower-layer Froude-number) over the sill region based on the two-layer approximation defined by the zero velocity surface for the cases; a) BASE=>LHM and b) HHM=>BASE, regions with $F^2 < 0.2$ are excluded.

Among these six experiments; we see that, for only the two of them; HHM=>BASE and BASE=>LHM, corresponding to the restarted solutions with decreased K_h values, the model can be considered to be slightly unsuccessful in switching to the LE equivalents due to the significant differences in the salinity responses within the reservoirs and slightly different results within the channel. For the rest of the experiments the difference between the switched and the LE solutions is insignificant. Actually, for these two cases the difference between the LE and the switched solutions is not only limited with the salinity responses within the reservoirs, but also these solutions display at least slightly unsteady responses while persisting a slow but continuous change of salinity stratification at the reservoirs at the final time-level of the model, Figure 6. For these two restarted cases, HHM=>BASE and BASE=>LHM (from high frictional to low-frictional state), the switched maximal-exchange solution is distinctively different than the initial steady-state solution, the model is able to adjust the exchange according to the this new solution successfully within the region from south-exit to the sill according to the nature of the maximal-exchange phenomenon where the information can only propagate away from this region. However, we know that the solutions developed under the influence of the boundary conditions are dependent on the initial level of the salinity interface within the reservoirs, reaching a steady-state solution either with a maximal-exchange response or with the drowned control conditions at the south-exit or at the sill, Sözer & Özsoy (2017). When the adjustment is not started from an already achieved steady-state, the governing solution and the driving forces, density difference for instance, are in a mutual interaction and shaping each other, thus an unsteady response due to an inconsistency is not observed. For the switched state solutions from one controlled solution to another, since the steady-state conditions did not develop together with this feedback, the possibility of an unsteady-solution is possible and observed in these two experiments due to the significant difference between the initialization and the equivalent LE

solution. This unsteady response is not observed for the BASE=>HHM despite the significant difference between the steady-state solutions of the BASE and HHM cases owing to the direction of less frictional to more frictional transition. The lack of this unsteady behavior for the restarted solutions with reduced K_v values is possibly due to the less significant effect of K_v on the two-layer exchange flow for the investigated parameter range.

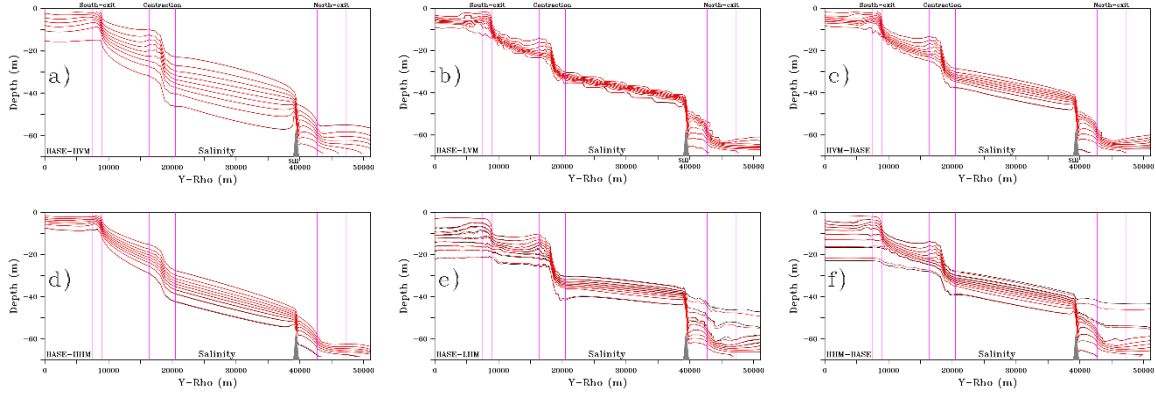


Figure 6. Comparison of the along-channel laterally averaged salinity for the last two time-levels (with the very same contour levels), Day=1.62 (red) and Day=2.02 (black), of the solutions; a) BASE=>HVM, b) BASE=>LVM c) HVM=>BASE, d) BASE=>HHM, e) BASE=>LHM and f) HHM=>BASE.

4. Conclusions

In this sensitivity study, a three-dimensional numerical ocean model's ability in switching from one steady-state to another, from a less frictional case to a more frictional one or vice versa, was investigated for the case of an idealized Bosphorus Strait model. The model can be considered as successful in switching from a less frictional state to a more frictional one, which is quite predictable due to the direction of the frictional change. However the model response when a steady-state solution of a well-mixed frictional simulation is restarted with reduced mixing coefficients is not obvious. The model is not successful in switching from higher to lesser horizontal mixing state and can be considered as partially successful for the cases where the vertical mixing is reduced which is probably due to the less significant effect of K_v on the flow for the investigated parameter range.

This sensitivity study test is aimed to be helpful in two aspects, the first one is based on a realistic physical phenomenon; e.g. how the dynamics of the flow responds while recovering from a strongly altered vertical stratification due to a strong wind over a short period. The second one aims to test whether the numeric of the model is able to switch between solutions of different frictional configurations correctly, which will be important in the realistic simulations with real topography and hydrography where the model is driven to the intended solutions by successive restarts in order to reduce the computational cost of a Bosphorus Strait model.

References

1. Altıok H, Sur H İ & Yüce H (2012). Variation of the cold intermediate water in the Black Sea exit of the Strait of İstanbul (Bosphorus) and its transfer through the strait. *Oceanologia* **54**(2): 233.
2. Altıok H, Sur H İ, Müftüoğlu A E & Yüce H (2010). Temperature, Salinity, and Flow Variations in the Strait of İstanbul (Bosphorus), in 2010-Rapp. Comm. Int. Mer Medit., vol. 39, p. 85, CIESM Congress (Venice 2010), CIESM: Mediterranean Science Commission, Monaco.
3. Andersen J J E C & Carmack E C (1984). Observations of Chemical and Physical Fine-structure in a Strong Pycnocline, Sea of Marmara. *Deep-Sea Res.*, **2**: 877-886.
4. Arakawa A & Lamb V R (1977). Methods of computational physics. *New York: Academic Press* **17**: 173-265.
5. Aydoğdu A, Pınardı N, Özsoy E, Danabasoglu G, Gürses Ö & Karspeck A (2018). Circulation of the Turkish Straits System under interannual atmospheric forcing. *Ocean Science* **14**: 99-1019.
6. Beşiktepe Ş, Özsoy E, Latif M A & Oğuz T (2000). Marmara Denizi'nin hidrografisi ve Dolaşımı, (Hydrography and Circulation of the Marmara Sea). Marmara Sea 2000 Symposium, İstanbul, Nov. 11-12, 2000, 14 pp.
7. Beşiktepe Ş, Özsoy E & Ünlüata Ü (1993). Filling of the Marmara Sea by the Dardanelles lower layer inflow. *Deep Sea Research Part I: Oceanographic Research Papers* **40**(9): 1815-1838.
8. Beşiktepe Ş T, Sur H İ, Özsoy E, Latif M A, Oğuz T & Ünlüata Ü (1994). The circulation and hydrography of the Marmara Sea. *Progress in Oceanography* **34**(4): 285-334.
9. Budgell W P (2005). Numerical simulation of ice-ocean variability in the Barents Sea region. *Ocean Dynamics* **55**(3-4): 370-387.
10. Büyükkay M (1989). The surface and internal oscillations in the Bosphorus, related to meteorological forces. M. Sc. Thesis, Institute of Marine Sciences, Middle East Technical University, Erdemli, İçel, Turkey, 169s.
11. Çetin N (1999). Analysis of the exchange flow through the Bosphorus Strait. Diss. M. Sc. Thesis, Institute of Marine Sciences, METU, Erdemli, Mersin.
12. Defant, A. (1961). *Physical Oceanography*. Pergamon Press, London, 1961. Vol. 1, pp. xvi + 729; Vol. 2, pp. Viii + 598.
13. Durski S M, Glenn S M & Haidvogel D B (2004). Vertical mixing schemes in the coastal ocean: Comparison of the level 2.5 Mellor-Yamada scheme with an enhanced version of the K profile parameterization. *Journal of Geophysical Research: Oceans* **109**(C1).
14. Farmer D M & Armi L (1986). Maximal two-layer exchange over a sill and through the combination of a sill and contraction with barotropic flow. *Journal of Fluid Mechanics* **164**:53-76.
15. Fennel K, Wilkin J, Levin J, Moisan J, O'Reilly J & Haidvogel D (2006). Nitrogen cycling in the Middle Atlantic Bight: Results from a three-dimensional model and implications for the North Atlantic nitrogen budget. *Global Biogeochemical*

Cycles **20**(3).

16. Gregg M C & Özsoy E (2002). Flow, water mass changes, and hydraulics in the Bosphorus. *Journal of Geophysical Research: Oceans* **107**(C3).
17. Griffies S M & Hallberg R W (2000). Biharmonic friction with a Smagorinsky-like viscosity for use in large-scale eddy-permitting ocean models. *Monthly Weather Review* **128**(8): 2935-2946.
18. Gunnerson C G & Özturgut E (1974). The Bosphorus. In: The Black Sea-Geology, Chemistry, and Biology (eds. Degens, ET and Ross, DA). *American Association of Petroleum Mem.* **20**: 99-115.
19. Haidvogel DB, Arango HG, Hedström K, Beckmann A, Malanotte-Rizzoli P & Shchepetkin AF (2000). Model evaluation experiments in the North Atlantic Basin: simulations in nonlinear terrain-following coordinates. *Dynamics of Atmospheres and Oceans* **32**(3): 239-281.
20. Hedström K S (2009). DRAFT Technical Manual for a Coupled Sea-Ice. *Ocean Circulation Model (Version 3), US Department of the Interior, Mineral Management Service, Anchorage, Alaska, Arctic Region Supercomputing Center, University of Alaska Fairbanks, Contract M07PC13368.*
21. Jarosz E, Teague W J, Book J W & Beşiktepe Ş (2011). Observed volume fluxes in the Bosphorus Strait. *Geophysical Research Letters* **38**(21).
22. Large W G, McWilliams J C & Doney S C (1994). Oceanic vertical mixing: A review and a model with a nonlocal boundary layer parameterization. *Reviews of Geophysics* **32**(4): 363-403.
23. Latif M A., Özsoy E, Oğuz T & Ünlüata Ü (1991). Observations of the Mediterranean inflow into the Black Sea. *Deep Sea Research Part A. Oceanographic Research Papers* **38**: 711-723.
24. Marsigli L F (1681). Osservazioni intorno al Bosforo Tracio overo Canale di Constantinopoli rappresentate in lettera all sacra real maesta di Cristina Regina di Svezia, Roma, 108p.
25. Mellor G L & Yamada T (1982). Development of a turbulence closure model for geophysical fluid problems. *Reviews of Geophysics* **20**(4): 851-875.
26. Oğuz T (2005). Hydraulic adjustments of the Bosphorus exchange flow. *Geophysical research letters* **32**(6).
27. Orlanski I (1976). A simple boundary condition for unbounded hyperbolic flows. *Journal of computational physics* **21**(3): 251-269
28. Ovchinnikov I M, Popov, Yu I (1991). Evolution of the Cold Intermediate Layer in the Black Sea. *Oceanology* **27**: 555-560.
29. Özsoy E & Ünlüata Ü (1997). Oceanography of the Black Sea: a review of some recent results. *Earth-Science Reviews* **42**(4): 231-272.
30. Özsoy E, Di Iorio D, Gregg M C & Backhaus J O (2001). Mixing in the Bosphorus Strait and the Black Sea continental shelf: observations and a model of the dense water outflow. *Journal of marine systems* **31**(1): 99-135.
31. Özsoy E, Latif M A, Beşiktepe S, Çetin N, Gregg M C, Belokopytov Goryachkin Y & Diaconu V (1998). The Bosphorus Strait: Exchange Fluxes, Currents and Sea-Level Changes. *NATO Science Series 2 Environmental Security* **47**(2): 1-28.
32. Özsoy E, Latif M A, Sur H İ & Goryachkin Y (1996). A review of the exchange flow

- regime and mixing in the Bosphorus strait. *Bulletin-Institut Oceanographique Monaco-Numero Special* 187-204.
33. Öztürk M, Ayat B, Aydoğan B & Yüksel Y (2012). 3D Numerical Modeling of Stratified Flows: Case Study of the Bosphorus Strait. *Journal of Waterway, Port, Coastal, and Ocean Engineering* **138**(5): 406-419.
 34. Peneva E, Stanev E, Belokopytov V & Le Traon P Y (2001). Water transport in the Bosphorus Straits estimated from hydro-meteorological and altimeter data: seasonal to decadal variability. *Journal of Marine Systems* **31**(1): 21-33.
 35. Pinardi N (2009). Misurare il mare: Luigi Ferdinando Marsili nell'Egeo e nel Bosforo, *Bononia University Press* 1679-1680.
 36. Raymond W H, Kuo H L (1984). A radiation boundary condition for multi-dimensional flows. *Quarterly Journal of the Royal Meteorological Society* **110**(464): 535-551.
 37. Sannino G, Sözer A & Özsoy E (2017). A high-resolution modelling study of the Turkish Straits System. *Ocean Dynamics* **67**(3-4): 397-432.
 38. Smagorinsky J (1963). General circulation experiments with the primitive equations: I. the basic experiment. *Monthly weather review* **91**(3): 99-164.
 39. Smolarkiewicz P K (2006). Multidimensional positive definite advection transport algorithm: an overview. *International journal for numerical methods in fluids* **50**(10): 1123-1144.
 40. Soffientino B & Pilson M E Q (2005). The Bosphorus Strait. A Special Place in the History of Oceanography. *Oceanography* **18**(2): 16-23.
 41. Song Y, & Haidvogel D (1994). A semi-implicit ocean circulation model using a generalized topography-following coordinate system. *Journal of Computational Physics* **115**(1): 228-244.
 42. Sözer A & Özsoy E (2002). A three-dimensional model of Bosphorus Strait dynamics. In *The 2nd Meeting on the Physical Oceanography of Sea Straits, Villefranche, 15th* (pp. 207-210).
 43. Sözer A (2013). *Numerical modeling of the bosphorus exchange flow dynamics* (Doctoral dissertation, Ph. D. thesis, Institute of Marine Sciences, Middle East Technical University, Erdemli, Mersin, Turkey).
 44. Sözer A, Özsoy E (2017). Modeling of the Bosphorus exchange flow dynamics. *Ocean dynamics* **67**(3-4): 321-343.
 45. Stanev E V, Grashorn S & Zhang Y J (2017). Cascading ocean basins: numerical simulations of the circulation and interbasin exchange in the Azov-Black-Marmara-Mediterranean Seas system. *Ocean Dynamics* **67**(8): 1003-1025.
 46. Tolmazin D (1985). Changing coastal oceanography of the Black Sea II: Mediterranean effluent. *Progress in oceanography* **15**(4): 277-316.
 47. Tuğrul S, Beşiktepe T & Salihoğlu I (2002). Nutrient exchange fluxes between the Aegean and Black Seas through the Marmara Sea. *Mediterranean Marine Science* **3**(1): 33-42.
 48. Umlauf L & Burchard H (2003). A generic length-scale equation for geophysical turbulence models. *Journal of Marine Research* **61**(2): 235-265.
 49. Ünlüata Ü, Oğuz T, Latif M A & Özsoy E (1990). On the physical oceanography of the Turkish Straits. In *The physical oceanography of sea straits* (pp. 25-60). Springer Netherlands.

50. Warner J C, Sherwood C R, Arango H G & Signell R P (2005). Performance of four turbulence closure models implemented using a generic length scale method. *Ocean Modeling* **8**(1): 81-113.
51. Wilkin J L, Arango H G, Haidvogel D B, Lichtenwalner C, Glenn S M & Hedström K S (2005). A regional ocean modeling system for the Long-term Ecosystem Observatory. *Journal of Geophysical Research: Oceans* **110**(C6).